Journal of Physics D: Applied Physics

PAPER • **OPEN ACCESS**

Surface acoustic waves as a sensitive probe for photoresponsive polarization memory in $SrTiO_3$

To cite this article: Y Uzun *et al* 2020 *J. Phys. D: Appl. Phys.* **53** 335301

OPEN ACCESS
IOP Publishing
Journal of Physics D: Applied Physics
J. Phys. D: Appl. Phys. **53** (2020) 335301 (7pp)
https://doi.org/10.1088/1361-6463/ab8a91

Surface acoustic waves as a sensitive probe for photoresponsive polarization memory in $SrTiO_3$

Y Uzun[1], I Gurbuz[1,2], M P De Jong[1] and W G Van Der Wiel[1]

[1] MESA+ Institute for Nanotechnology, University of Twente, PO Box 217, 7500, AE Enschede, The Netherlands
[2] Material Science and Nanoengineering Department, Sabanci University, Istanbul, Turkey

E-mail: m.p.dejong@utwente.nl

Received 27 January 2020, revised 13 March 2020
Accepted for publication 17 April 2020
Published 4 June 2020

Abstract

Transient electric polarization in single crystalline $SrTiO_3$ (STO) substrates was studied by measuring the transmission of surface acoustic waves (SAWs). We applied a large dc electric field (8×10^6 Vm^{-1}) to interdigital transducers (IDTs) on STO substrates in order to induce local piezoelectricity, which is required to generate and transmit SAWs. The resulting electric polarization and the retention thereof were analyzed as a function of time after the applied electric field was removed, by measuring transient SAW signals. The retained polarization turned out to provide strong electromechanical coupling, comparable to that resulting from the dc-field-induced piezoelectricity. SAW signals were observed for more than 30 h (in absence of an external dc electric field), which is evidence for a long-lasting retention of electric polarization. Remarkably, this polarization was found to be rapidly suppressed as the sample was exposed to visible light. By measuring the transient SAW transmission under illumination with light at different wavelengths, we identified photoconductivity and/or acceleration of oxygen vacancy migration by photon-induced splitting of bound vacancy pairs as the main mechanisms behind this photoresponsive memory effect.

Supplementary material for this article is available online

Keywords: complex-oxides, surface acoustic waves, electric polarization, photoconductivity

(Some figures may appear in colour only in the online journal)

1. Introduction

Among the innumerous intriguing features of $SrTiO_3$ (STO), one of the most debated is ferroelectricity [1]. The crystal structure of STO is very similar to that of native ferroelectrics such as $Pb[Zr_xTi_{1-x}]O_3$ (PZT) and $BaTiO_3$ (BTO), however STO is a cubic and hence centro-symmetric crystal, while the aforementioned ferroelectric materials are tetragonal, orthorhombic, or rhombohedral (depending on composition and thin film properties) [2, 3]. Hence, spontaneous polarization is observed in PZT and BTO, whereas this is not the case for native STO at room temperature. The ferroelectric Curie temperature of STO is ~ 105 K [4, 5]. Below this temperature, STO experiences a structural phase transition from cubic to tetragonal, such that the inversion symmetry is broken and spontaneous polarization is induced. At much lower temperatures another phase transition occurs where the ferroelectric phase is suppressed due to quantum fluctuations [6]. Therefore, STO is known as an incipient ferroelectric material. Nevertheless, under certain conditions, room temperature ferroelectricity has been demonstrated in STO by inducing

strain in the lattice, i.e. by doping or growing in thin film form on lattice mismatched substrates [1, 7–15]. There are other effects, involving the spatial separation of charged defects under influence of an external electric field, that can also lead to long-lasting, ferroelectric-like, polarization in STO [16, 17]. In particular, oxygen vacancies, which are unavoidably present in STO, may play a role in such effects.

In this work, we report on a ferroelectric-like, photoresponsive electric polarization memory effect in STO single crystals at room temperature and at 150 K. We use surface acoustic wave (SAW) generation in STO as a sensitive probe for residual polarization in the near surface region. We note in passing that these investigations originated from our work on acoustoelectric coupling between SAWs and electrons confined in $LaAlO_3$/STO two-dimensional electron systems [18]. SAW generation requires piezoelectricity, which can be induced in STO by applying an external dc electric field [19, 20]: Due to the ionic nature of STO, comprising Sr^{2+}, Ti^{4+} cations and O^{2-} anions, an electric field displaces these charges in opposite directions and thus, the lattice inversion symmetry is broken and a polarization is induced [17]. This approach has been used to excite surface acoustic waves (SAWs) on STO substrates [21–23]. We detect the retention of this polarization after the dc bias is removed, by measuring transient SAW signals. Remarkably, the SAW signal intensity directly after removing the dc bias is comparable to that with the dc bias still applied, which shows that the retained polarization in STO provides robust electromechanical coupling.

We employ SAW devices comprising two inter-digital transducers (IDTs) in the delay line configuration on single crystalline STO substrates. A dc voltage is applied to the IDTs to create a polarization in STO and hence 'program' the memory, which is subsequently read out by measuring the SAW transmission upon applying an rf-signal. When an rf-signal is applied to a metallic inter-digital transducer (IDT) deposited on a piezoelectric (or ferroelectric) substrate or thin film, the inverse piezoelectric effect induces a dynamic strain field that propagates (mainly as Rayleigh waves) at the sound velocity and can be detected by a second IDT via the piezoelectric effect, converting the strain wave back into an electrical signal. By the help of this process, our particular aim is to understand the retention and relaxation process of polarization in STO after the dc electric field is removed, using the effect of light illumination on a polarized STO substrate, at photon wavelengths of 375 nm, 405 nm and 600 nm. We find that the retention time depends strongly on the wavelength and optical power used. Based on these findings, we conclude that the transient electric polarization in STO is mainly due to oxygen vacancy migration, and is thus not ferroelectric in nature.

2. Experimental details

Measurements were carried out on a device as shown in figure 1(a), in the dark and in high vacuum, using a four-probe low temperature probe station. Two of the four probes were configured as rf lines and connected to IDTs through a vector network analyzer (VNA). The remaining two probes were used to mount and electrically connect an LED. IDT1 and IDT2 were connected to a VNA through a bias tee, which divides rf and dc lines via an internal capacitor, enabling biasing the rf signal via an external dc source while protecting the rf signal generator (VNA). The IDTs are designed in the double finger configuration with 20 μm periodicity, and fabricated as a Cr/Al/Cr multilayer stack with a total thickness of 100 nm. The two IDTs in a delay line device are 500 μm apart and deposited directly on top of the single crystalline STO substrate by e-beam evaporation. When a dc voltage is applied to an IDT, the ionic lattice beneath the IDT is deformed as depicted in figure 1(b), due to the displacement of Sr^{2+}, Ti^{4+} cations and O^{2-} anions towards negatively and positively charged IDT fingers, respectively. The lattice deformation and its associated polarization is increased by applying higher voltages. The breakdown voltage varies from device to device and is 40–50 V for short experiments (several minutes), while extended/repeated biasing could lead to breakdown at lower voltages as well. Therefore, we adopted a safe maximum bias voltage of 20 V for both IDTs, which corresponds to a maximum electric field of $8 \cdot 10^6$ Vm^{-1}, ensuring reproducibility of a large number of measurements on the same device. In order to generate SAWs, a 0 dBm rf signal is always applied together with the dc bias voltage.

3. Results and discussions

We first measured SAW generation and detection on an STO substrate under application of 20 V dc-bias. After that we analyzed the time-evolution of SAW signals when the dc-bias was switched off and the sample was left for relaxation. Measurements were performed in the dark and were compared to experiments in which we exposed the sample to light with different wavelengths during the relaxation process. All measurements were done both at room temperature and at 150 K. In order to avoid any effects due to the crystal phase transition at 105 K, we kept the STO sample temperature well above this value.

As shown in figure 1(d) (red curve), when a 20 V dc bias was applied to both IDTs at the same time, SAW transmission was measured at 657 MHz corresponding to the 3rd harmonic resonance frequency of the device. As the bias was switched off, the SAW transmission amplitude decreased strongly (blue) but remained finite, which shows that a finite polarization is retained in the STO. This memory effect becomes much more pronounced at 150 K, as seen in figure 1(e). Under application of 20 V dc bias on both IDTs, SAW transmission is again observed at 150 K, with an increased intensity as compared to the room temperature experiment, due to (i) the increased dielectric constant and thus higher electrostriction and (ii) reduced phonon scattering during SAW transmission [21, 24–26]. In addition, the resonance frequency of the device shifted to 665 MHz at 150 K, due to the increase in sound velocity of the medium at lower temperatures [27]. The highly pronounced SAW transmission signal remaining after the dc bias was switched off shows that the induced polarization in

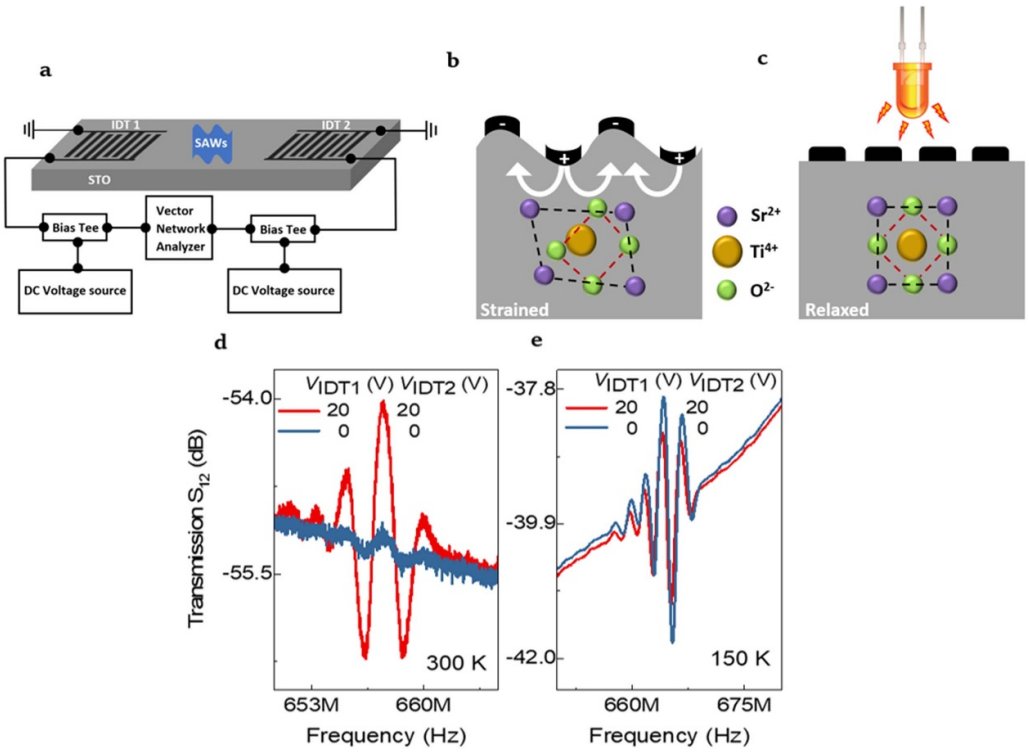

Figure 1. SAW transmission on a non-piezoelectric STO substrate. (a) Schematic representation of a SAW device on an STO substrate and the measurement set-up. RF input signals were biased via external dc voltage sources in order to induce local piezoelectricity beneath the IDTs. (b) Cross sectional view of a strained STO substrate (grey) under application of a dc bias to the IDT (black). White arrows represent the electric field lines, which dislocate cations (purple and dark yellow) and anions (green) in the lattice, breaking the inversion symmetry, as shown schematically. (c) Relaxation of the strained STO, under light exposure using an LED emitting photons with a wavelength of 375 nm, 405 nm or 600 nm. (d) Room temperature transmission of 3rd harmonic SAWs on STO, when 20 V dc bias was applied to IDT1 and IDT2 (red), and measured as soon as the dc bias was switched off for both IDTs (blue). (e) 3rd harmonic SAWs measured at 150 K under the same conditions.

the crystal structure of STO (figure 1(b)) is retained: as the rf signal is continuously applied, SAWs are generated even in absence of a dc bias, as in conventional piezoelectric or ferroelectric materials.

In the following, the relaxation time or, in other words, the electric polarization memory of the polarized STO was analyzed under zero dc bias, in the dark and in high vacuum. Upon polarizing a dielectric like STO in an electric field, strain and deformation results as ions are displaced from their equilibrium positions. After switching off the electric field, the material returns to its initial, unpolarized state, in which case we expect the SAW generation and transmission to disappear. However, our results show a very different behavior.

In figure 2, the SAW transmission on an STO substrate is shown as a function of time after switching off the applied dc electric field, at room temperature and 150 K. The red curves in figures 2(a) and (c) are copies of the blue curves of figures 1(d) and (e), other measurements in these figures represent the evolution of the SAW transmission in time, under a continuously applied rf input signal. As shown in figure 2(b), SAW transmission above the noise level could be detected for about 10 h at room temperature, and for more than 30 h at 150 K, as seen in figure 2(d). After 30 h at 150 K, a clear SAW transmission signal was still present, and complete disappearance of this signal may be expected to take much longer. This demonstrates a long lasting, strong polarization in the crystal after the dc bias was switched off, which is uncommon in ordinary dielectrics.

Figure 3 shows the SAW transmission as a function of time measured during polarization decay stimulated by illumination with light, using LEDs with various output wavelengths and optical powers (see supplementary information for details about LED characteristics). The LEDs were mounted (one at a time) inside the measurement chamber but were thermally isolated from the cooling stage onto which the SAW device was mounted. The temperature of the LED was thus kept constant at room temperature. In figures 3(a)–(c), the effects of light exposure on SAW transmission are shown for illumination wavelengths of 375 nm, 405 nm and 600 nm, respectively, under various optical output powers.

A comparison of the results obtained for different wavelengths is shown in figure 3(d). Every data point represents the peak value of the SAW transmission signal. In figure 3(a), the optical output power was tuned by changing the applied forward bias current to a 375 nm LED, which corresponds to a photon energy of 3.31 eV, higher than the STO band gap of 3.2 eV [28, 29]. Under these illumination conditions, the depolarization is fast even at low output power of the LED ($\ll 100\ \mu$W), therefore we operated the LED at very low bias currents for which no precise output power value is known (see figure S1(a) (available online at

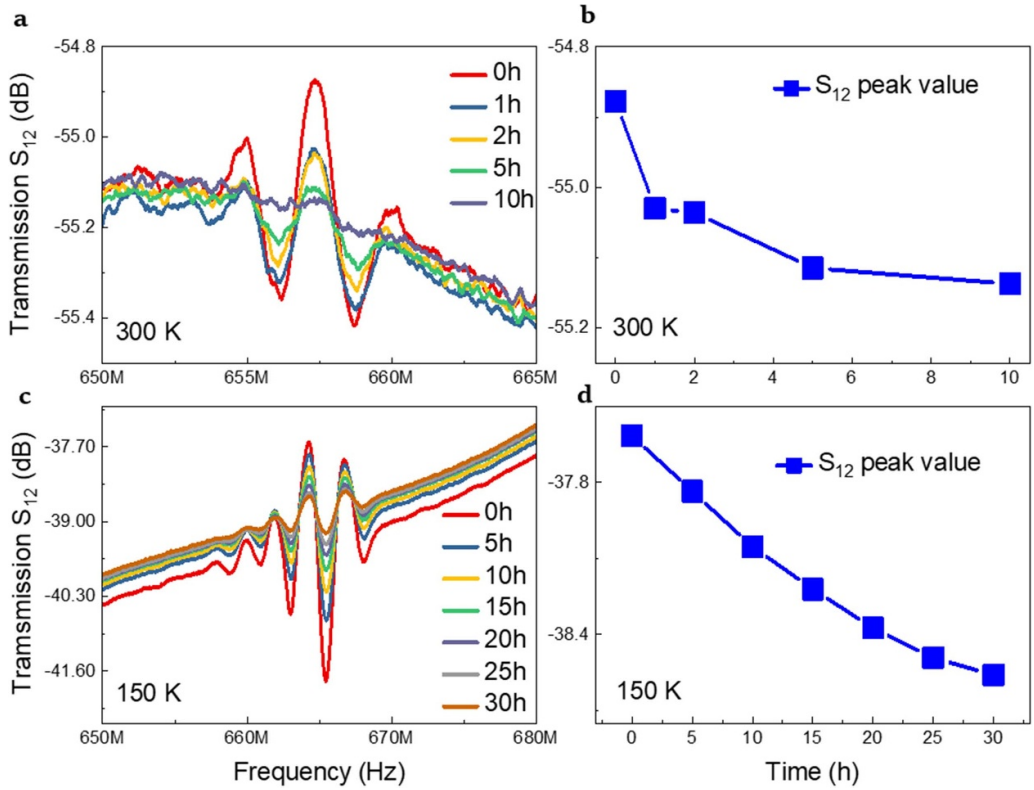

Figure 2. Electric field induced polarization memory of STO at room temperature and 150 K. (a) Evolution of SAW transmission signal as a function of time at room temperature after the dc bias is switched off on both IDTs. (b) Peak values of the transmission signals of figure 2(a), as a function of time. (c) Evolution of SAW transmission signal as a function of time at 150 K after the dc bias is switched off on both IDTs. (d) Peak values of the transmission signals of figure 2(c), as a function of time.

stacks.iop.org/JPhysD/53/335301/mmedia) in supplementary material, for details). Initially a 150 μA bias current was applied to the LED and the SAW transmission was recorded every 10 s. In the first 30 s, only a very small decrease in transmission was observed, and after that a rapid decay was measured. Over the next 50 s the SAW signal disappeared. As the applied bias current was increased to 250 μA, the transmission decay time decreased to 20 s, however a very similar decay profile was measured. Further increasing the bias current (and hence optical output power) results in faster decay of the SAW transmission. At $\approx$ 500 μA, the decay time is about equal to the minimum time required to measure the SAW transmission ($\approx$1 s). As shown, in the first 2 s, a very small decay was measured, after which the signal disappeared in less than 1 s. In figures 3(b) and (c), results are shown for similar experiments with 405 nm and 600 nm LEDs, corresponding to 3.06 eV and 2.07 eV photon energy, both smaller than the band gap of STO. For the 405 nm LED, 20, 50, 100 and 125 μW optical output powers were used while the SAW transmission was measured. Rapid decay was observed as soon as the sample was exposed to light,resulting in complete suppression within 125 s for the lowest output power.

As the output power was increased sequentially, similar decay profiles were obtained in 50, 30 and 18 s, respectively. In figure 3(c), transient SAW signals are shown for illumination with a 600 nm LED, using optical output powers of; 50 μW, 100 μW, 125 μW and 250 μW. The obtained decay profile was again similar to that for illumination with the 405 nm LED (figure 3(b)). The inset shows the same data on a logarithmic time scale. The quasi linear trend of the SAW signals versus time on a double log-scale suggest a power-law decay consistent with thermal relaxation processes [9, 30]. The same trend was also obtained for other LED wavelengths. For sub-band-gap excitation (405 and 600 nm LEDs), the suppression of SAW signals occurs on a much longer time scale than for above-band-gap excitation (375 nm LED), for comparable optical output power of the LEDs. Similar decay curves are obtained for all measurements, with longer decay times observed for either a longer wavelength or lower optical output power.

In figure 3(d), a comparison is shown of the effects of LED illumination at different wavelengths on the SAW transmission decay time. A 100 μW optical output power was used for the 405 nm and 600 nm LEDs. The 375 nm LED was operated at 500 μA forward bias, yielding a low optical output power $\ll$100 μW (see supplementary material for details) but nevertheless a very fast decay of the SAW transmission, (just within the limits of our measurement setup). The comparison in figure 3(d) clearly shows that the SAW transmission decays faster as the LED wavelength decreases and the photon energy increases.

We now discuss possible mechanisms that explain the observed effects. We attribute the loss of SAW transmission to the (stimulated) relaxation of residual electric

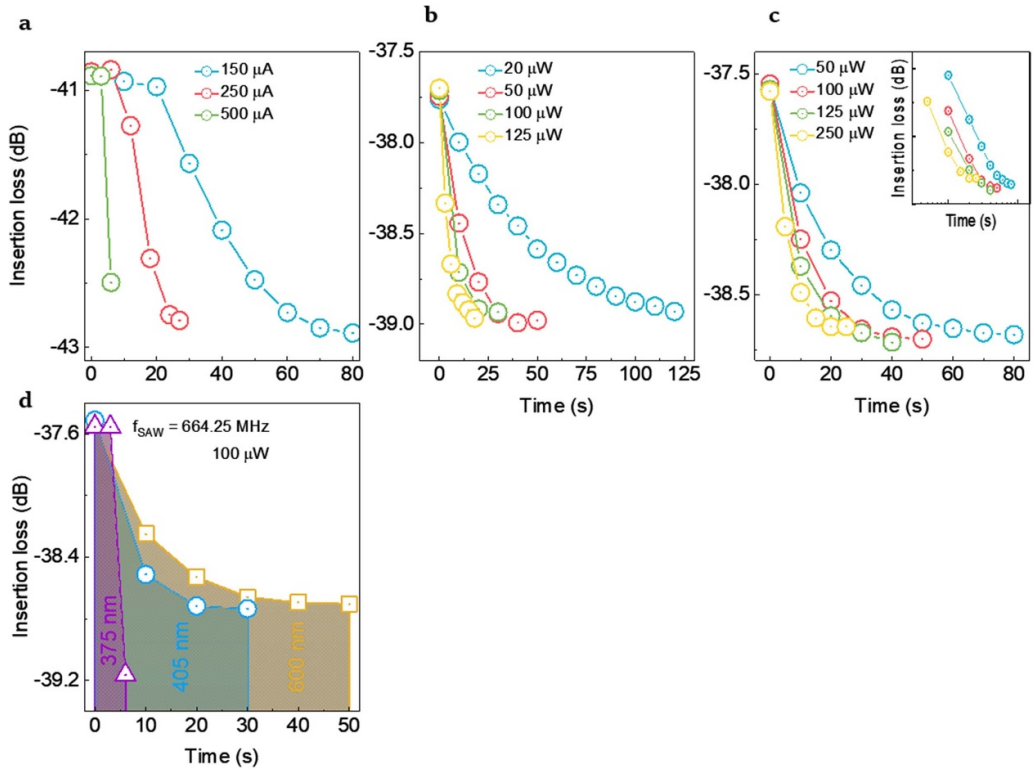

Figure 3. Relaxation of SAW transmission in STO at 150 K under illumination with light with (a), 375 nm (b), 400 nm and (c), 600 nm wavelength at various optical output powers. The inset in (c) shows the decay curves on a logarithmic time scale. (d) SAW transmission under illumination with 375 nm (purple), 405 nm (blue), and 600 nm (yellow) LEDs. For comparison, 100 μW optical output power was used for the 405 nm and 600 nm LEDs, while 500 μA forward bias was used for 375 nm LED. Note that this corresponds to a much smaller optical output power (100 μW is obtained at 5 mA forward bias on the 375 nm LED, see supplementary material for details).

polarization to the unpolarized ground state. There are two different mechanisms that could be responsible for such a behavior according to previous reports. One is photoconductivity, which is a consequence of electron excitation to the conduction band from the valance band due to absorption of photons with an energy higher than the optical band gap [28]. The other is accelerated oxygen vacancy migration under illumination with visible light [30]. Migration of charged defects such as oxygen vacancies under application of an electric field contributes to the polarization of STO, where the timescale for saturation of the polarization should depend on the mobility of the oxygen vacancies and the applied field strength [29]. Depolarization after removal of the electric field is expected to occur on a much longer timescale, since the only driving forces for this depolarization are the much weaker residual electric field (which opposes the polarization) and the concentration gradient of oxygen vacancies. This is consistent with our observation of a slow decay of SAW signals in the dark, acting as a measure of polarization in STO, upon removal of the dc electric field (figures 2(b) and (d)), whilst the signals appear immediately after applying a dc bias.

STO is a band insulator with a band gap of 3.2 eV. When the sample is exposed to 375 nm light, which has 3.31 eV photon energy, free electrons are generated in the material (photoconductivity), which rapidly screen any residual polarization such that the SAW signal disappears. As the optical output power is increased, by increasing the forward bias current through the LED, more electrons are excited per unit time and the decay time of SAW transmission decreases accordingly. However, photoconductivity is not a valid explanation for the effects shown in figures 3(b) and (c), as the photon energies (3.06 eV and 2.07 eV) used in these experiments are smaller than STO band gap. Excitation of electrons across the band gap is therefore not possible, only in-gap (defect) states could give rise to photon absorption and subsequently trigger depolarization [31]. As reported previously, oxygen vacancy migration is accelerated when STO is exposed to visible light, with a photon energy smaller than the band gap of STO [32]. It is known that oxygen vacancies in STO form bound pairs. Upon optical excitation of electrons residing in vacancy pair states (to localized anti-bonding orbitals or to the conduction band), the immobile pairs are destabilized and can split into two mobile unbound vacancies, which accelerates the relaxation towards the initial unpolarized state [33, 34]. This process thus speeds up the complete relaxation of the crystal to the point where no SAWs are generated.

Additional support for the discussion given above is provided by measurements of the photocurrent and two point probe resistance between the ground (G) and signal (S) pads of an IDT. Here, in every measurement 10 mV bias was applied to the device, which then generated ~29 pA background current in the dark. The measured photocurrent and resistance values, as well as the optical output powers of the LEDs, are given in

Table 1. Measured photocurrent and resistance values of an IDT at 10 mV dc bias voltage, under the illumination by different wavelength LEDs (correspond to figure S2 in supplementary material). The values represent the saturation current, measured after transient effects had vanished. Dark-current values were subtracted from the photocurrent.

λ (nm)	Optical power or bias current (μA for 400 nm and 600 nm)	Photocurrent (pA)	Resistance (MΩ)
375	• 150	• 21	• 200
	• 250	• 21	• 200
	• 500	• 31	• 170
400	• 20	• 8	• 270
	• 50	• 9	• 260
	• 100	• 13	• 240
	• 125	• 16	• 230
600	• 5	• 0	• 350
	• 10	• 0	• 350
	• 125	• 0	• 350
	• 250	• 0	• 350

table 1. Detailed information regarding the LED characteristics is provided in figure S2 in the supplementary material.

These results confirm that the photon-induced relaxation of polarization in the STO single crystal involves the generation of mobile charge carriers, resulting in a finite photocurrent. Due to the bandgap of STO, significant photoconductivity is only observed under illumination with UV light, i.e. for the 375 nm LED where we obtained up to a 31 pA photocurrent at optical power $\ll$100 μW. For sub-band-gap excitation, e.g. using the 405 and 600 nm LEDs, the generated current is much smaller at optical power $\approx$100 μW. As the wavelength of the LEDs is increased, only charged vacancy migration, or electrons excited from in-gap states to the conduction band, can contribute to the photocurrent.

4. Conclusion

We have used SAW generation and detection as a sensitive probe for transient polarization in STO single crystals after application of a dc electric field of $8 \cdot 10^6$ Vm^{-1}. SAW transmission, which relies on induced piezoelectricity on STO and hence is a measure of electric polarization, was observed for over 30 h after the removal of the dc electric field. This ferroelectric-like, transient polarization turned out to be very susceptible to illumination with light, even for photon energies smaller than the band gap of STO. This strongly points to charged oxygen vacancies, and their accelerated migration by photon-induced splitting of bound vacancy pairs, as a source for transient electric polarization in STO, and contributes to the understanding of ferroelectric-like behavior in (the near-surface region of) STO single crystals. In addition, our approach regarding SAW transmission on intrinsically non-piezoelectric STO substrates and the associated photoresponsive memory effect are promising for using STO substrates in device applications that would ordinarily require piezoelectric or ferroelectric materials. In particular, the very long polarization memory (more than 30 h) and fast response of the SAW signals to light (on the order of 1 s) opens up unique possibilities to use similar devices in memory or optical sensor applications.

Acknowledgments

The authors would like to thank M. Bayraktar for discussions. This project was financially supported by the European Union's Horizon 2020 research and innovation programme under the Marie Skłodowska-Curie grant agreement No. 642688 (SAWtrain). The authors also acknowledge financial support of the Netherlands Organisation for Scientific Research (NWO) through a Vrij Programma grant (QUAKE, 680.92.18.04/7566).

ORCID iDs

Y Uzun https://orcid.org/0000-0001-9756-0319
M P De Jong https://orcid.org/0000-0003-3668-9121
W G Van Der Wiel https://orcid.org/0000-0002-3479-8853

References

[1] Lee D *et al* 2015 *Science* **349** 1314
[2] Von Hippel A 1950 *Rev. Mod. Phys.* **22** 221
[3] Tra V T *et al* 2013 *Adv. Mater.* **25** 3357
[4] Erba A, El-Kelany K E, Ferrero M, Baraille I and Rérat M 2013 *Phys. Rev.* B **88** 035102
[5] Grupp D E and Goldman A M 1997 *Science* **276** 392
[6] Salje E K H, Aktas O, Carpenter M A, Laguta V V and Scott J F 2013 *Phys. Rev. Lett.* **111** 247603
[7] Warusawithana M P *et al* 2009 *Science* **324** 367
[8] Huang M, Bi F, Bark C W, Ryu S, Cho K H, Eom C B and Levy J 2014 *Appl. Phys. Lett.* **104** 161606
[9] Jang H W *et al* 2010 *Phys. Rev. Lett.* **104** 197601
[10] Bark C W *et al* 2012 *Nano Lett.* **12** 1765
[11] Biegalski M D, Jia Y, Schlom D G, Trolier-Mckinstry S, Streiffer S K, Sherman V, Uecker R and Reiche P 2006 *Appl. Phys. Lett.* **88** 192907
[12] Haeni J H *et al* 2004 *Nature* **430** 758
[13] Junquera J and Ghosez P 2003 *Nature* **422** 506
[14] Tikhomirov O, Jiang H and Levy J 2002 *Phys. Rev. Lett.* **89** 147601
[15] Zhong W L, Wang Y G, Zhang P L and Qu B D 1994 *Phys. Rev. B* **50** 698

[16] Freeman J R, Kallmann H P and Silver M 1961 *Rev. Mod. Phys.* **33** 553
[17] Sihvonen Y T 1967 *J. Phys. D: Appl. Phys.* **38** 4431
[18] Uzun Y, Smink A E M, De Jong M P, Hilgenkamp H and Van Der Wiel W G 2020 *Appl. Phys. Lett.* **116** 011601
[19] Li F, Jin L, Xu Z and Zhang S 2014 *Appl. Phys. Rev.* **1** 011103
[20] Morito K, Iwazaki Y, Suzuki T and Fujimoto M 2003 *J. Phys. D: Appl. Phys.* **94** 5199
[21] Iamsakun K 1972 *Electron. Lett.* **8** 555
[22] Iamsakun K, Elder W, Wilkinson C D W and La Rue R M D 1975 *J. Phys. D: Appl. Phys.* **8** 266
[23] Alzuaga S, Daniau W, Salut R, Baron T, Ballandras S and Defay E 2014 *Appl. Phys. Lett.* **105** 062901
[24] Weaver H E 1959 *J. Phys. Chem. Solids* **11** 274
[25] Neville R C, Hoeneisen B and Mead C A 1972 *J. Phys. D: Appl. Phys.* **43** 2124
[26] Kuleev I G, Kuleev I I and Arapova I Y 2007 *Phys. Solid State* **49** 1335
[27] Bjerkan L and Fossheim K 1977 *Solid State Commun.* **21** 1147
[28] Saadatkia P, Stepanov P and Selim F A 2018 *Mater. Res. Express* **5** 016202
[29] Poole V M, Jokela S J and McCluskey M D 2017 *Sci. Rep.* **7** 6659
[30] Fondado A, Mira J and Rivas J 2005 *Phys. Rev.* B **72** 024302
[31] Hanzig J, Mehner E, Jachalke S, Hanzig F, Zschornak M, Richter C, Leisegang T, Stöcker H and Meyer D C 2015 *New J. Phys.* **17** 023036
[32] Hanzig J *et al* 2013 *Phys. Rev.* B **88** 024104
[33] Li Y, Lei Y, Shen B G and Sun J R 2015 *Sci. Rep.* **5** 14576
[34] Lei Y *et al* 2014 *Nat. Commun.* **5** 5554